Polymer 51 (2010) 4103–4109

Contents lists available at ScienceDirect

Polymer

journal homepage: www.elsevier.com/locate/polymer

Interactions of binary liquid mixtures with polysaccharides studied using multi-dimensional NMR relaxation time measurements

J. Kolz [a], Y. Yarovoy [b], J. Mitchell [a], M.L. Johns [a,*], L.F. Gladden [a]

[a] Magnetic Resonance Research Centre, Department of Chemical Engineering and Biotechnology, University of Cambridge, Pembroke Street, Cambridge, CB2 3RA, UK
[b] Unilever R&D, NA 40 Merritt Boulevard, Trumbull, CT 06611, USA

ARTICLE INFO

Article history:
Received 1 April 2010
Received in revised form
30 June 2010
Accepted 2 July 2010
Available online 3 August 2010

Keywords:
Starch
Water–glycerol mixture
T_2–T_2 exchange

ABSTRACT

Nuclear magnetic resonance transverse T_2 relaxation time has proven to be a valuable parameter for characterizing liquid/polymer interactions. This measurement is applicable to many food, personal care, and cosmetic products that contain multi-component liquid mixtures. Here, we investigate the interactions of corn starch with water/glycerol mixtures of different weight compositions and explore liquid exchange dynamics; such a system is relevant to the personal care industry. We use a combination of chemical shift resolved ^{1}H T_2 relaxation measurements and corresponding two-dimensional T_2 relaxation exchange experiments using both a conventional experimental protocol and a modified method with the addition of NMR chemical shift selectivity. Two relaxation regimes were evident for the hydroxyl ^{1}H (found in both water and glycerol) whilst three relaxation regimes are evident for the aliphatic glycerol ^{1}H associated here with strongly bound, weakly bound, and free (bulk) liquid, respectively. At higher water contents preferential absorption of glycerol was evident. T_2–T_2 exchange maps with a range of storage times reveal molecular exchange rates between all three regimes due to self-diffusion. Rapid exchange of water between the bulk and bound locations was evident in the case of pure water. Exchange rates for hydroxyl ^{1}H was considerably reduced by the inclusion of glycerol.

1. Introduction

Polysaccharides such as corn starch are encountered in a wide range of food, cosmetics, and personal care products. In most of these product formulations, the interaction between the starch and liquid components is an essential aspect of the product performance. Due to the importance of these interactions, many studies utilising a variety of different techniques have been carried out to investigate the liquid–starch interactions. For example, differential scanning calorimetry (DSC) was used to study gelatinization, phase transitions and water dynamics in water/starch mixtures [1–6]. Infrared spectroscopy techniques were applied to study structural changes and phase transitions of starch [7] as well as the study of 'short-range' water–starch interactions [8] during gelatinzation [9] (hydration and a crystalline to amorphous phase transition) and retrogradation [10] (recrystallization and dehydration). Rheological measurements [11], X-ray scattering, and small angle neutron scattering (SANS) have also been applied to study the structure [4,12] and water distribution [13] within starch granules. From these studies, it was determined that starch granules exhibit alternating layers of crystalline and amorphous lamellae (referred to as the semi-crystalline stack) surrounded by amorphous material. On combination with excess water, the water enters the amorphous growth ring, resulting in swelling of the starch; at low concentrations, water also acts as a plasticizer. Upon heating gelatinization (break-down of starch molecules to allow additional water adsorption) occurs, although the semi-crystalline stack remains unaltered until destabilised by even higher temperatures.

Nuclear magnetic resonance (NMR) has proven to be a valuable tool in studying starch/water interactions with either solid state spectroscopy or time-domain relaxation measurements. Solid state NMR has been used extensively to study the structure and morphology of native and modified starch applying predominantly magic angle spinning (MAS) techniques in combination with cross-polarization [14–20]. The different states of water in starch granules have also been identified using time-domain NMR analyses; specifically T_1 and T_2 relaxation times [21–25]. These studies provided evidence that water exists in different states within the starch granules, characterised by discrete T_2 relaxation times. However, the physical interpretation of these water states is still open to debate. Tang et al. [25] studied the distribution of water in packed beds of water saturated starch granules, assigning the

* Corresponding author.
E-mail address: mlj21@cam.ac.uk (M.L. Johns).

0032-3861/$ – see front matter © 2010 Elsevier Ltd. All rights reserved.
doi:10.1016/j.polymer.2010.07.004

different relaxation time components to interstitial water, water located in the amorphous growths rings, and water located in the semi-crystalline lamellas. Rapid diffusive exchange between the water in the amorphous growth rings and the semi-crystalline lamella prevented the observation of distinct T_2 peaks in the measured distribution at room temperature (290 K), these emerged at lower temperatures (277 K) as a consequence of a reduced self-diffusion coefficient. Le Botlan et al. used NMR relaxation analysis to quantify the different relaxation time components assigning them to water strongly and weakly bound in wheat starch [24]. Chatakanonda et al. [21] used distributions of T_2^* obtained from free induction decay (FID) measurements [26] as well as deuterium broad-line spectroscopy on starch samples with low water content, differentiating between mobile and immobile water (i.e., weakly and tightly bound water), and suggesting that the weakly bound water might exist in channels between the crystalline domains. This suite of NMR relaxation techniques was used to study the effects of gelatinization [23,27–29] and retrogradation [30,31] processes on the distribution of water in the different states within the starch granules. Time-domain NMR techniques have also been applied to the study of the microscopic distribution of water in food products containing starch, such as bread [32–34], dough [35,36], or potatoes [37], while spatially resolved magnetic resonance imaging (MRI) techniques were employed to study water distributions in food products on a macroscopic scale [38,39].

Multi-dimensional relaxation time distributions can offer additional insights into structure and molecular motion. They allow relaxation times T_1 and T_2, or self-diffusion coefficient D, to be correlated. The development of an efficient numerical method for solving first-order Fredholm integrals with tensor product structure [40] enabled the implementation of the data analysis on standard desktop computers. Since then, T_1–T_2, T_2–T_2, and D–T_2 correlation and exchange experiments have been used extensively in the study of liquid saturated porous media such as reservoir rocks [41–43], cementitious building materials [44,45], and catalysts [46].

In this work we are concerned primarily with applications of relaxation correlation and exchange measurements in soft matter and liquid–liquid systems. Previously, T_1–T_2 and T_2–T_2 experiments have been applied extensively to food products [47–50]. Other applications include cross-linked natural rubbers [51] and surfactant solutions [52]. In some of these works, and in studies of sucrose solutions [53] and cellular structures in carrots [54], chemical sensitivity was incorporated into the measurements in order to help identify components in the correlation plots. Recently, chemical sensitivity was added efficiently to this suite of measurements in the form of T_2–T_1–δ correlation and T_1–T_1–δ exchange experiments (where δ is the chemical shift) by acquiring chemical spectra and T_1 relaxation information simultaneously [55]. However, other chemically resolved correlations such as T_2–T_2–δ cannot be implemented in the same manner; each data point must be determined separately, thus requiring considerably longer acquisition times than the standard T_2–T_2 experiment.

The focus of the literature relevant to the work presented here has been exclusively on the interaction between water and starch: a combination encountered commonly in food products. In this paper we consider the interaction of a binary liquid mixture of water and glycerol with starch granules. This particular combination of materials is encountered in a variety of personal care products where the glycerol is added to act as a plasticizer and moisturizer. We employ a combination of NMR techniques to gain new insights into the processes governing absorption of water and glycerol by the starch granules and subsequence exchange of the water and the glycerol between different domains both within and external to the starch granules; in this manner we consider the relative exchange and absorption characteristics of the water and glycerol with respect to the starch granules. The NMR experiments used include multi-dimensional relaxation measurements that enable diffusive molecular exchange between different relaxation domains in the system to be explored. We also modify the multi-dimensional relaxation measurements by inclusion of a chemically selective saturation pulse enabling isolation of the signal from a particular NMR resonance peak; this affords the method an enhanced chemical selectivity at no additional total acquisition time cost.

2. Experimental

The native corn starch granules used in all the experiments were supplied by Unilever research, Trumbull, CT, USA, and had a mean diameter of 15 μm. A number of water/glycerol/starch samples were prepared with different water/glycerol ratios. Glycerol (>99.0 wt.% purity) was obtained from Acros Organics, UK. Two series of samples were prepared: Series 1 (hereafter referred to as samples A1–E1) had a constant liquid-to-starch mass ratio of 1:1, and Series 2 (hereafter referred to as samples A2–E2) had a constant liquid-to-starch ratio of 2:1. The water-to-glycerol ratios of the individual samples (A–E) are detailed in Table 1. The mixtures were poured into 5 mm diameter glass tubes and allowed to settle for at least 24 h, during which time sedimentation of the starch granules occurred. All mixtures showed an excess liquid phase indicating the starch granules were saturated. For the NMR measurements, the samples were positioned in the radio frequency (rf) resonator so that signal was detected only from the liquid/starch phase and not the excess liquid phase.

All the NMR measurements were conducted on a Bruker DMX spectrometer with a 7.14 T vertical-bore superconducting magnet and a 15 mm internal diameter rf birdcage resonator operating at 300 MHz for ^{1}H (which was used exclusively). Typical rf pulse durations were $t_{90} = 15$ μs and $t_{180} = 30$ μs, corresponding to tip angles of 90° and 180°, respectively. The NMR pulse sequences employed are described below.

A standard chemically resolved Carr-Purcell Meiboom-Gill (CPMG) [56,57] echo train was used with an echo spacing of $t_E = 500$ μs to encode T_2 relaxation times. A 90° rf pulse is used to excite the spin ensemble prior to the application of a series of 180° rf refocusing pulses. Between each 180° pulse, the spins form an echo. The signal from the final echo in the train was acquired and Fourier transformed to provide a chemical shift resolved spectrum. The number of refocusing pulses was varied logarithmically between $n = 2$ to 1024 echoes in 32 steps. A standard inversion recovery pulse sequence [58] was utilised to encode T_1 relaxation times, where the recovery times were incremented logarithmically between $t_R = 1$ ms–10 s in 32 steps. The spin ensemble is inverted initially with a 180° rf pulse, then interrogated after time t_R by a 90° rf pulse. Again, chemical shift resolution was obtained by Fourier transform of the detected signal (FID). Distributions of T_2 and T_1 relaxation times were obtained by inverting the Fredholm integrals describing the exponential decay or recovery, respectively [59]. An

Table 1
Initial ratios of water and glycerol in the different samples. (both Series 1 and 2)

Sample	Water content/wt.%	Glycerol content/wt.%
A	100	0
B	75	25
C	50	50
D	25	75
E	0	100

optimum solution was obtained using the generalized cross validation method (GCV) [60].

T_2–T_2 exchange maps were acquired using the pulse sequence shown in Fig. 1(a), with exchange or storage times ranging from t_s = 10–600 ms; the echo spacing was t_E = 500 μs. The pulse sequence comprises two CPMG echo trains separated by a stimulated echo [61] that stores the spins on the z-axis for a time t_s. Data is acquired only from the second CPMG train and reconstructed to form the two data dimensions. In the first (indirect) dimension the number of echoes was varied from m = 1 to 128 in separate acquisitions, while in the second (direct) dimension the number of echoes was fixed at n = 1024 echoes. The phase and amplitude of the magnetization at the centre of each echo in the direct dimension was acquired. Only the even echoes were used for data processing since rf pulse errors are cancelled in the even echoes. The total T_2 relaxation times were t_A in the first dimension and t_B in the second dimension; T_1 recovery occurs during the storage time t_s. In order to perform the two-dimensional numerical inversion [40], it is necessary first to compress the data and kernel functions describing the exponential decays in each dimension using singular value decompositions (SVD). The compressed data is then fitted to the expected form (kernel functions) using an optimised minimization, where the best fit is again determined by the GCV method. This conventional T_2–T_2 protocol was applied to samples A1, B1, and C1.

Fig. 1(b) shows a modification to the T_2–T_2 exchange experiment: the inclusion of a chemically selective saturation pulse during the storage interval of the pulse sequence. This enables selected spectral resonance lines to be saturated so that signal is detected only from the remaining resonance lines. This modification has no impact on the total acquisition time. This sequence was applied to sample C1 with a frequency-selective half-Gaussian shaped 90° rf pulse with a duration of t_{90} = 3.2 ms inserted during the exchange interval. The frequency range of the saturation pulse was varied to correspond to, and hence eliminate signal from, either the hydroxyl or the aliphatic resonance peak (see below). All the other experimental parameters in the modified T_2–T_2 exchange measurement were identical to those used in the basic T_2–T_2 sequence described above.

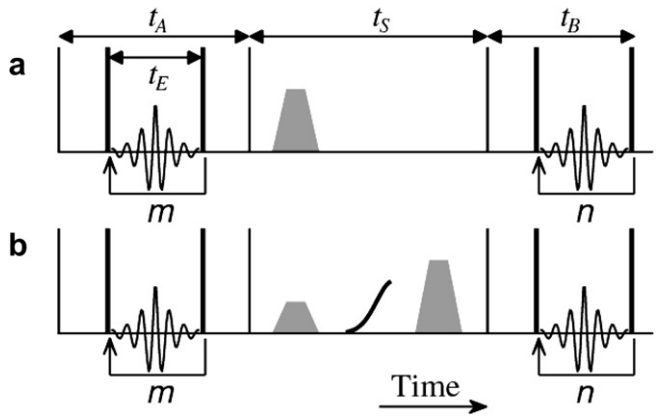

Fig. 1. Pulse sequence for the T_2–T_2 exchange measurements. The standard experiment (a) comprises two CPMG encoding intervals of duration t_A and t_B. The number of echoes acquired in each interval is m and n, respectively. The spins are stored on the z-axis for a time t_S. A homospoil magnetic field gradient (grey trapezoid) is applied to dephase coherent spins remaining in the x–y plane. The thin and thick vertical bars represent 90° and 180° rf pulses, respectively. The modified sequence (b) has chemical selectivity introduced via a half-Gaussian rf pulse applied during the z-storage interval to saturate the spins that are not required. A second homospoil gradient is added to dephase these spins; this has a different amplitude to the first homospoil gradient to prevent the formation of a gradient echo.

3. Results and discussion

3.1. 1D spectral analysis

NMR ^{1}H chemical spectra (as shown in Fig. 2), obtained from the various samples exhibited, typically, two distinct resonances, peaks corresponding to hydroxyl (OH) and aliphatic (CH) ^{1}H resonance, with the exception of samples A1 and A2 that had only a single peak corresponding to OH as expected. The OH resonance peak originates from both the water and the glycerol, which will be in rapid chemical exchange (exchange time ~1 ms) [62] and thus indistinguishable in the experiments used here, whilst the CH resonance peaks originates from the glycerol alone. The absence of CH resonance peaks in samples A1 and A2 indicate that the CH resonance peaks in the other samples originated only from glycerol and not from 'mobilised' starch. The ratio of the OH and CH resonance peaks in the samples agreed to within 3% (and in most cases less than 1%) with the known water-to-glycerol ratio. These observations suggested that the starch did not contribute significantly to the NMR signal; this conclusion was further confirmed by replacing the water with D_2O, where minimal signal was detected.

3.2. 1D T_2 relaxation analysis

Fig. 3 shows the T_2 distributions obtained by inversion of the CPMG data acquired from (a) samples A1 to E1 for the OH resonance peak and (b) samples B1 to E1 for the CH resonance peak.

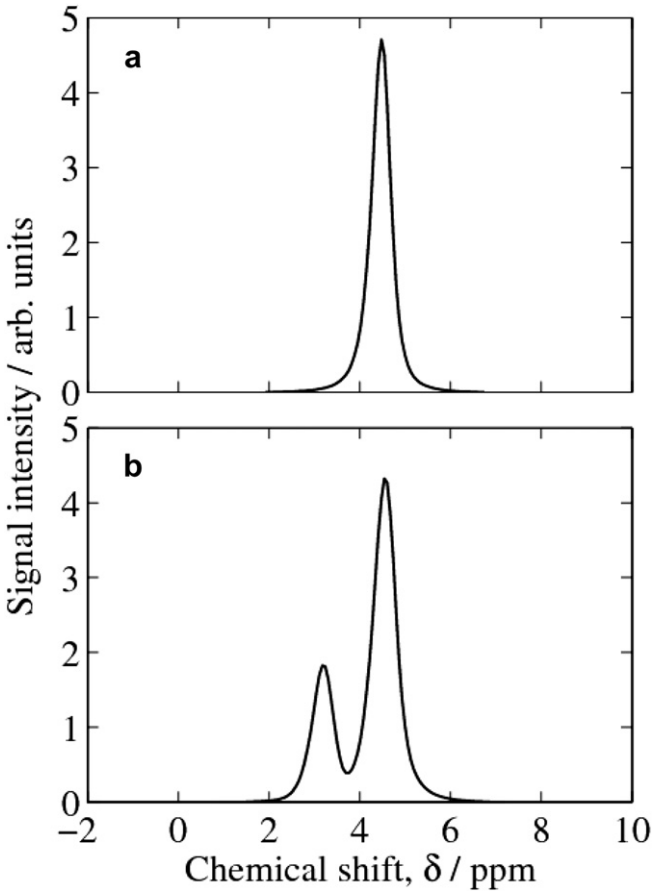

Fig. 2. ^{1}H spectra obtained from samples (a) A1 and (b) C1. Sample A1 contains only water plus starch and has a single OH resonance at δ = 4.5 ppm. Sample C1 contains glycerol and water plus starch, and exhibits two resonance lines corresponding to OH at δ = 4.5 ppm and CH at δ = 3.2 ppm.

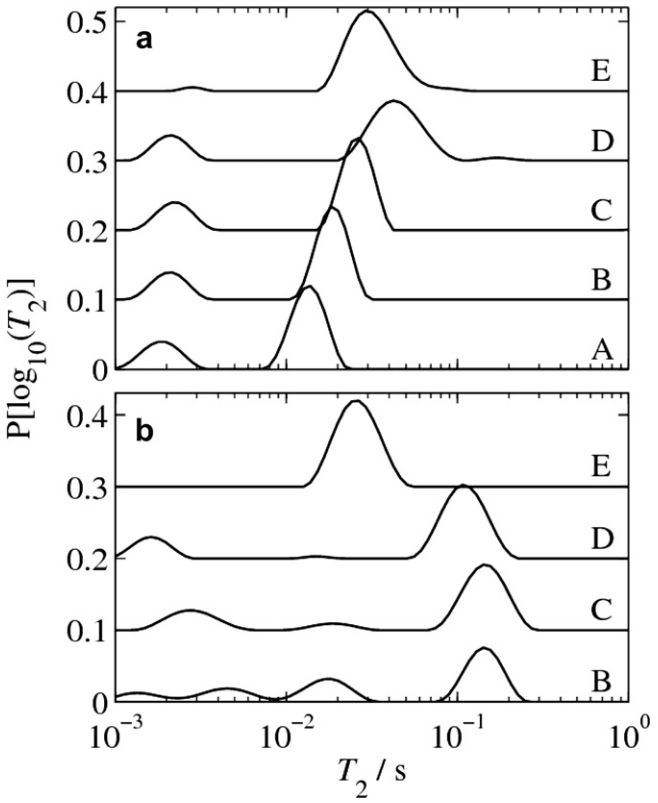

Fig. 3. Stack plots of one-dimensional T_2 distributions obtained for the (a) OH resonance and (b) CH resonance. The T_2 distributions were acquired from samples with different water-to-glycerol ratios. The water fractions were (a) 0, 25, 50, 75, and 100% (top to bottom), and (b) 0, 25, 50, and 75% (top to bottom). The sample names (A–E) are shown in the plots.

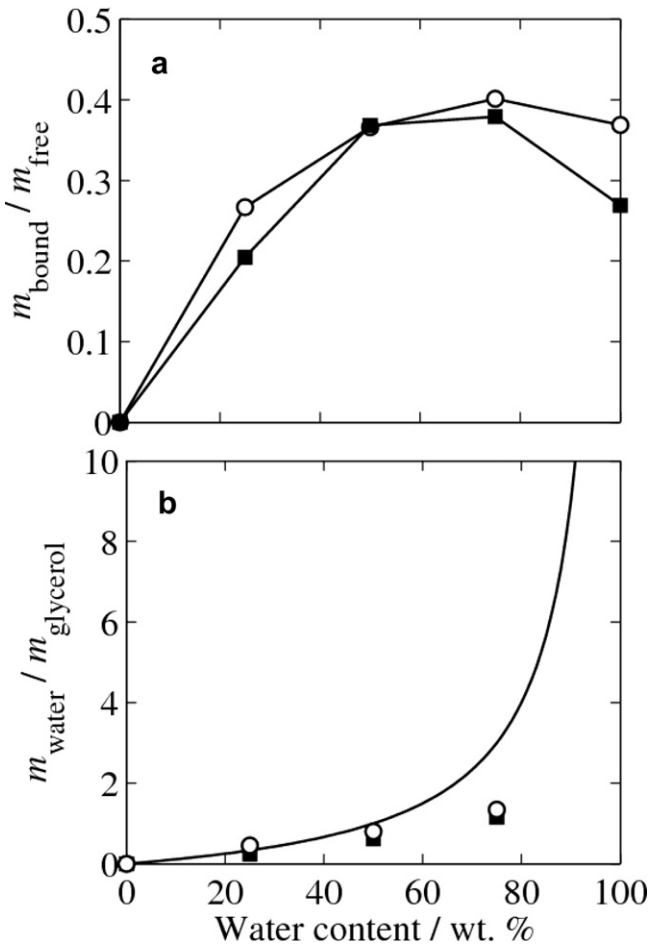

Fig. 4. (a) Mass ratio of absorbed versus free liquid and (b) mass ratios of water-to-glycerol for the absorbed component, determined from the T_2 distributions in Fig. 3. These ratios were determined for Series 1 (open circles) and Series 2 (solid squares). In Fig. 3(b), the solid line indicates the original mass ratio of water-to-glycerol added to the starch.

Two distinct relaxation time components (evident as distinct peaks) are observed typically in the T_2 distributions for the OH resonance in Fig. 3(a). The short relaxation time component was centred consistently on $T_2 = 1.8$ ms for samples A1 to D1, whereas the long relaxation time component varied from $T_2 \approx 14$–42 ms as the water content decreased. We associate the two observed T_2 components with two different physical domains in which the OH groups are located. The short T_2 component is assigned to liquid bound to the starch particles, while the long T_2 component is assigned to free diffusing interstitial liquid. At room temperature this interpretation is consistent with previous literature [24], where distinct peaks for tightly bound and weakly bound water only emerged at lower temperatures; these were assigned to water associated with semi-crystalline and amorphous regions of the starch respectively. Sample E1, containing no added water, exhibited a dominant relaxation time component centred on $T_2 = 29.2$ ms, attributed to the slow diffusion of glycerol in the absence of water, a very low intensity short T_2 component was also evident at $T_2 = 2.8$ ms. This result suggests glycerol is effectively unable to form significant interactions with starch in the absence of water.

In Fig. 3(b), three T_2 components can be identified for the CH resonance in samples B1 to D1; the CH resonance derives exclusively from the glycerol content. The short T_2 component ($T_2 \leq 10$ ms) is associated with glycerol bound strongly to the starch; the intermediate T_2 component ($T_2 \approx 10$–50 ms) is associated with weakly bound or motionally restricted glycerol; the long T_2 component ($T_2 \approx 100$ ms) is associated with free diffusing glycerol in the interstitial void between the starch granules. The intermediate component is a weak peak but is reproducible for both Series 1 and 2. We speculate that the strongly and weakly bound components observed corresponds to glycerol in the semi-crystalline and amorphous domains of the starch, as observed previously for water at lower temperatures [24]. The comparatively lower diffusion coefficient of glycerol results in a reduced exchange rate between these domains and hence distinct peaks in the T_2 distribution. Sample E1 containing no water exhibits a different behaviour: only one component is observed centred on $T_2 \approx 25$ ms. This is consistent with the single dominant T_2 component observed for the OH resonance in this sample, see Fig. 3(a). The equivalent T_2 distributions were also obtained for samples A2 to E2 (not shown). The trends observed for Series 1, as discussed above, are reproduced consistently for Series 2. We conclude, therefore, that the addition of excess liquid does not alter the water/glycerol/starch interactions over the range considered.

Fig. 4(a) shows the mass ratio of bound to free liquid ($m_{\text{bound}}/m_{\text{free}}$) in the samples as a function of total water content. This was determined by appropriate integration of the OH and CH T_2 component peaks in Fig. 3. The amount of bound liquid is seen to progressively increase with total water content, and then decrease slightly in the case of pure water. Fig. 4(b) shows the mass ratio between water and glycerol ($m_{\text{water}}/m_{\text{glycerol}}$) for the bound liquid fraction as a function of the composition of the original liquid phase. The values were determined from:

$$\frac{m_{\text{water}}}{m_{\text{glycerol}}} = \frac{\frac{1}{2}\left(I_{\text{hyd}} - \frac{3}{5}I_{\text{ali}}\right)M_{\text{water}}}{\frac{1}{5}I_{\text{ali}}M_{\text{glycerol}}} \quad (1)$$

where I_{hyd} and I_{ali} are the integrals of the respective hydroxyl or aliphatic peaks in the T_2 distributions; M_{water} and M_{glycerol} are the molecular weights. The pre-factors originate from the type of functional group and hydrogen indices of water and glycerol; it is also necessary to account for the contribution of glycerol to both OH and CH resonances. The solid line in Fig. 4(b) shows the theoretical mass ratio for all the water and glycerol contained in the system. No preferential absorption of water or glycerol by the starch is observed for the system below an approximate water content of 50 wt.%. However, above this water content, a deviation is observed indicating preferential binding of the glycerol. A spectrum of the excess liquid above the starch packing was acquired for sample C1 (50 wt.% water); this revealed the same water-to-glycerol ratio as in the initial liquid mixture.

3.3. 2D T_2–T_2 relaxation analysis

A selection of two-dimensional T_2–T_2 exchange plots at a range of storage times (t_s) are shown in Fig. 5 for sample A1, containing only starch and water. Two peaks are observed on the $T_2^A = T_2^B$ diagonal, in agreement with the one-dimensional T_2 distributions in Fig. 3(a), and these correspond to bound (short T_2) and free water (long T_2). It is observed that off-diagonal exchange peaks are present, positioned symmetrically either side of the $T_2^A = T_2^B$ diagonal, even at the shortest storage time. This indicates rapid exchange between the bound and free water populations. As the storage time increases, the total signal intensity is reduced due to T_1 recovery; the relative size of the off-diagonal peaks increases however as expected due to exchange.

Fig. 6 contains a selection of T_2–T_2 exchange plots for sample C1, containing starch and a 1:1 wt mixture of water and glycerol. These plots were obtained without chemical selectivity, so signal from both the OH and CH resonances contribute. Here, three peaks are observed on the $T_2^A = T_2^B$ diagonal, in agreement with the sum of the one-dimensional T_2 distributions for the OH and CH resonances in Fig. 3(a) and (b). The shortest relaxation time component, $T_2 \approx 3$ ms, is attributed to strongly bound glycerol and bound water. The intermediate component, $T_2 \approx 30$ ms, is attributed to weakly bound glycerol and free water. The long relaxation time component, $T_2 \approx 200$ ms, is attributed to free glycerol only. At short storage times, $t_s = 10$ ms, a single pair of symmetric exchange peaks are observed, indicative of exchange between the short and intermediate relaxation time components. As the storage time is increased, additional exchange peaks are observed in Fig. 6(b) and (c), consistent with exchange between the short and long relaxation time components, and between the intermediate and long relaxation time components respectively. When these peaks are of low intensity, see Fig. 6(b), the position of the peaks is influenced by inversion errors (related to the signal-to-noise ratio) and exchange during encoding times t_A and t_B.

In all cases, the pairs of symmetric exchange peaks have near identical intensities. This suggests that, even though there are multiple exchange pathways, it is possible to analyse the data using the two-site exchange model given by Monteilhet et al. [45] For each exchange pathway, the ratio of exchange peak I_{XP} to total peak I_{TP} intensity is given as a function of storage time t_s. The peak intensities are determined by integrating over the region of interest in the T_2–T_2 exchange plots. Experimental and inversion errors are estimated by varying the size of the integral bounds as described in detail elsewhere [63]. The data are then fitted using the two-site exchange model which requires the initial relaxation

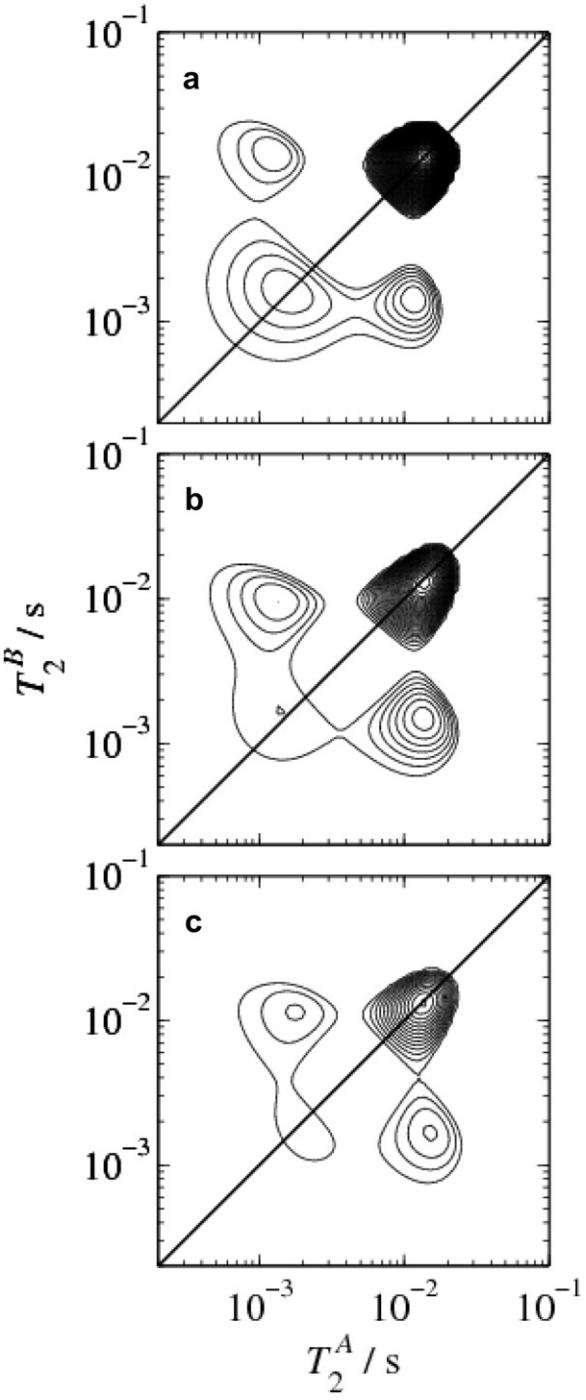

Fig. 5. T_2–T_2 exchange plots for sample A1 acquired with storage times of (a) $t_S = 10$ ms, (b) $t_S = 100$ ms, and (c) $t_S = 600$ ms. The solid diagonal line indicates $T_2^A = T_2^B$. In each plot, two main peaks and two exchange peaks are visible. The intensity of each plot decreases with increasing storage time due to T_1 relaxation. The contour intervals are the same in each plot.

times T_1 and T_2 (independent of exchange) and the relative size of the two spin populations. These parameters were estimates from the one-dimensional T_1 and T_2 data. For sample A1 (water only, thus only the OH resonance), a single exchange pathway was observed between bound and free water. The fit to the exchange data is shown in Fig. 7(a), where an exchange time of $t_x = 64$ ms was obtained. Assuming the mean diffusion coefficient of the water/glycerol mixture is $D_{\text{eff}} \sim 10^{-9}$ m^2 s^{-1} and using

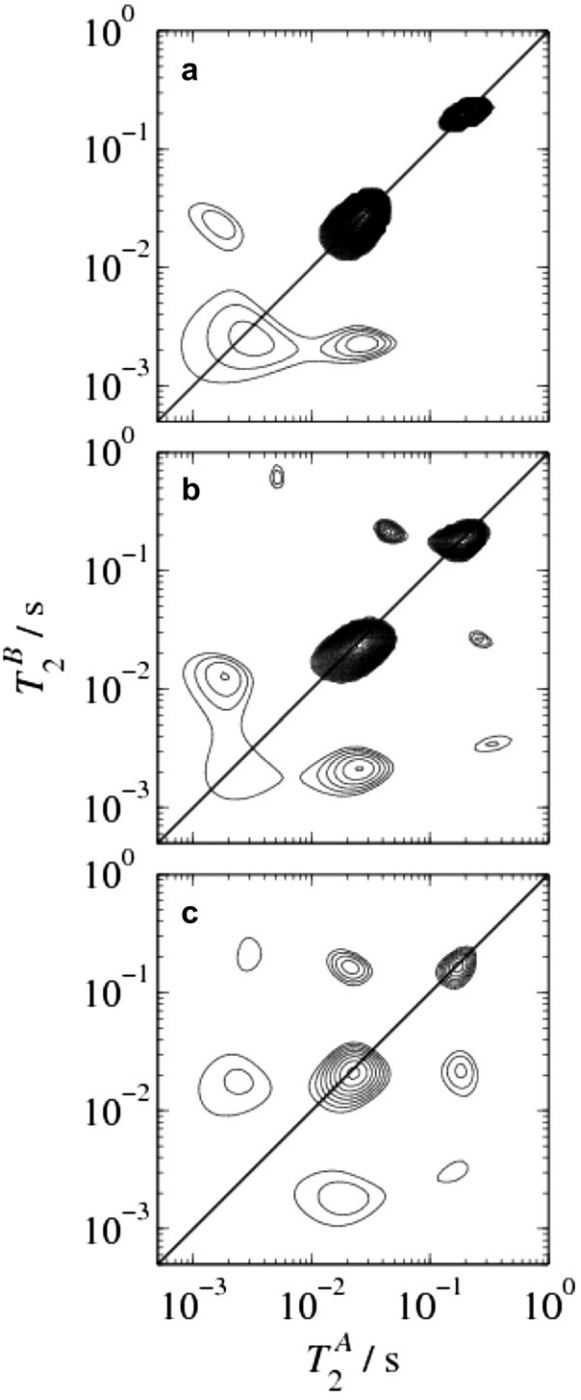

Fig. 6. T_2-T_2 exchange plots for sample C1 acquired with storage times of (a) $t_S = 10$ ms, (b) $t_S = 100$ ms, and (c) $t_S = 600$ ms. The solid diagonal line indicates $T_2^A = T_2^B$. In each plot, three main peaks are present, although in (c) the intensity of the shortest relaxation time component is too small to be visible. In (a), two exchange peaks are present. In (b) and (c) a total of six exchange peaks are evident. The intensity of each plot decreases with increasing storage time due to T_1 relaxation. The contour intervals are the same in each plot.

$x_{\text{exchange}} = \sqrt{6D_{\text{eff}}t_x}$ to estimate the exchange distance we get a value of 19 μm which is consistent with the mean un-swollen starch granule diameter of 15 μm and hence our assignment of bound and free water.

The exchange data for sample C1 (50 wt.% water) are shown in Fig. 7(b). Exchange between the short and intermediate T_2 peaks,

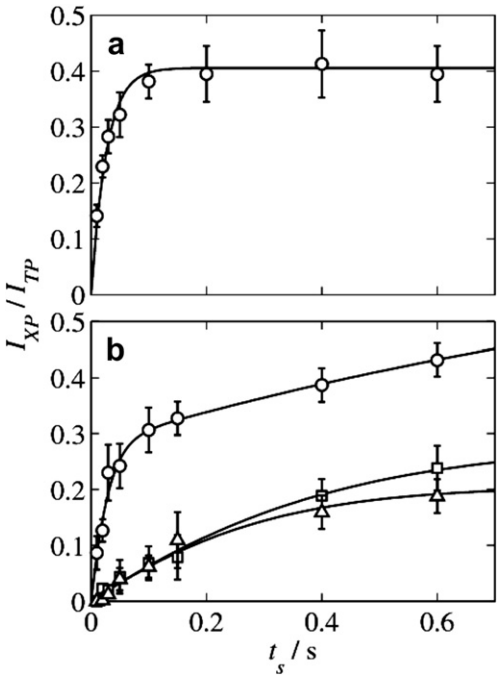

Fig. 7. Exchange plots showing the increase in the ratio of exchange peak I_{XP} to total peak I_{TP} intensity as a function of storage time t_S for samples (a) A1 and (b) C1. These data were determined from the corresponding T_2–T_2 exchange plots (see text for details). In (a) a single exchange pathway (circles) is present associated with bound/free water. In (b) three exchanges pathways are present associated with (circles) strongly bound/weakly bound glycerol and bound and free OH resonance, (squares) strongly bound/free glycerol, and (triangles) weakly bound/free glycerol. The solid lines represent a best fit to the exchange model of Monteilhet et al. [45].

Fig. 7(b, circles), exhibited two distinct exchange times determined as $t_x = 0.082$ and 3.20 s. This is consistent with the contribution of both free OH and weakly bound glycerol to the intermediate T_2 peak. The other two exchange pathways, Fig. 7(b, squares and triangles) occur between intra-granular glycerol (strongly or weakly bound) and inter-granular (free) glycerol. For exchange between strongly bound and free glycerol, Fig. 7(b, squares), $t_x = 1.45$ s; for exchange between weakly bound and free glycerol, Fig. 7(b, triangles), $t_x = 1.32$ s.

The observation of two distinct exchange times with respect to the exchange between the short and intermediate T_2 peaks in Fig. 7(b) is ambiguous in terms of which corresponded to exchange of the OH resonance and glycerol respectively. In order to assign these, the chemical shift selective T_2–T_2 exchange plots, as described above, were acquired. This allowed separation of the OH (in fast exchange between water and glycerol) and CH (exclusively glycerol) resonance contributions, which were analysed individually using the exchange model. This produced t_x values of 0.08 s and 2.65 s for the CH and OH resonances respectively with respect to exchange between the short and intermediate T_2 peaks. Thus the CH (exclusively glycerol) resonance is in rapid exchange consistent with the short length-scales separating weakly and strongly bound material (assigned to be semi-crystalline and amorphous regions respectively). Interestingly the presence of the glycerol has drastically lengthened the exchange time of the hydroxyl resonance relative to that of pure water. For completeness the exchange times for the CH resonance (glycerol) in these chemically resolved plots were 2.2 (free-strongly bound) and 1.5 s (free-weakly bound), broadly consistent with the corresponding data for the chemical shift unresolved results, as extracted from Fig. 7.

4. Conclusions

The interaction of various water/glycerol mixtures with starch was investigated with a range of techniques. Bulk relaxation measurements allowed determination of both the bound liquid fraction and the water/glycerol composition of that fraction as a function of total water content. Preferential absorption of glycerol was observed at higher water content. T_2–T_2 exchange plot were also acquired and revealed rapid exchange of the OH resonance in the case of pure water (which was broadly consistent with the starch granule size), this was substantially reduced when glycerol was present. This was facilitated by the use of a novel chemical shift spectral selection into these T_2–T_2 exchange plots, allowing unambiguous assignment of exchange rates for OH and CH contributions. Rapid exchange of glycerol between strongly and weakly bound sites was also observed. In future we will exploit this experimental protocol to explore these absorption and exchange rate characteristics as a function of temperature and hence starch structural modification.

References

[1] Biliaderis CG, Page CM, Maurice TJ, Juliano BO. J Agric Food Chem 1986;34 (1):6–14.
[2] Biliaderis CG, Maurice TJ, Vose JR. J Food Sci 1980;45(6):1669.
[3] Biliaderis CG. Food Chem 1983;10(4):239–65.
[4] Jenkins PJ, Donald AM. Carbohydr Res 1998;308(1–2):133–47.
[5] Kalichevsky MT, Jaroszkiewicz EM, Ablett S, Blanshard JMV, Lillford PJ. Carbohydr Polym 1992;18(2):77–88.
[6] Kim YS, Wiesenborn DP, Orr PH, Grant LA. J Food Sci 1995;60(5):1060–5.
[7] Capron I, Robert P, Colonna P, Brogly M, Planchot V. Carbohydr Polym 2007;68 (2):249–59.
[8] Rueda DR, Secall T, Bayer RK. Carbohydr Polym 1999;40(1):49–56.
[9] Wesley IJ, Blakeney AB. J Near Infrared Spect 2001;9(3):211–20.
[10] Ottenhof MA, Hill SE, Farhat IA. J Agric Food Chem 2005;53(3):631–8.
[11] Rao MA, Okechukwu PE, Da Silva PMS, Oliveira JC. Carbohydr Polym 1997;33 (4):273–83.
[12] Jenkins PJ, Donald AM. Polymer 1996;37(25):5559–68.
[13] Perry PA, Donald AM. Int J Biol Macromol 2000;28(1):31–9.
[14] Gidley MJ, Bociek SM. J Am Chem Soc 1988;110(12):3820–9.
[15] Kulik AS, Haverkamp J. Carbohydr Polym 1997;34(1–2):49–54.
[16] Li S, Dickinson LC, Chinachoti P. Cereal Chem 1996;73(6):736–43.
[17] Morgan KR, Furneaux RH, Larsen NG. Carbohydr Res 1995;276(2):387–99.
[18] Morgan KR, Furneaux RH, Stanley RA. Carbohydr Res 1992;235:15–22.
[19] Sivoli L, Perez E, Lares M, Leal E. Interciencia 2009;34(1):52–6.
[20] Tang HR, Hills BP. Biomacromolecules 2003;4(5):1269–76.
[21] Chatakanonda P, Dickinson LC, Chinachoti P. J Agric Food Chem 2003;51 (25):7445–9.
[22] Choi SG, Kerr WL. Food Res Int 2003;36(4):341–8.
[23] Choi SG, Kerr WL. Carbohydr Polym 2003;51(1):1–8.
[24] Le Botlan D, Rugraff Y, Martin C, Colonna P. Carbohydr Res 1998;308 (1–2):29–36.
[25] Tang HR, Godward J, Hills B. Carbohydr Polym 2000;43(4):375–87.
[26] Hahn EL. Phys Today 1953;4(November):4–9.
[27] Gonera A, Cornillon P. Starch-Starke 2002;54(11):508–16.
[28] Ritota M, Gianferri R, Bucci R, Brosio E. Food Chem 2008;110(1):14–22.
[29] Tananuwong K, Reid DS. Carbohydr Polym 2004;58(3):345–58.
[30] Choi SG, Kerr WL. Cereal Chem 2003;80(3):290–6.
[31] Lewen KS, Paeschke T, Reid J, Molitor P, Schmidt SJ. J Agric Food Chem 2003;51(8):2348–58.
[32] Lodi A, Abduljalil AM, Vodovotz Y. Magn Reson Imaging 2007;25 (10):1449–58.
[33] Lodi A, Tiziani S, Vodovotz Y. J Agric Food Chem 2007;55(14):5850–7.
[34] Wang X, Choi SG, Kerr WL. Lebensm-Wiss Technol 2004;37(3):377–84.
[35] Assifaoui A, Champion D, Chiotelli E, Verel A. Carbohydr Polym 2006;64 (2):197–204.
[36] Doona CJ, Baik MY. J Cereal Sci 2007;45(3):257–62.
[37] Micklander E, Thybo AK, van den Berg F. Lebensm-Wiss Technol 2008;41 (9):1710–9.
[38] Esselink EFJ, van Aalst H, Maliepaard M, van Duynhoven JPM. Cereal Chem 2003;80(4):396–403.
[39] MacMillan B, Hickey H, Newling B, Ramesh M, Balcom B. Food Res Int 2008;41 (6):676–81.
[40] Venkataramanan L, Song YQ, Hurlimann MD. IEEE Trans Signal Process 2002;50(5):1017–26.
[41] Hurlimann MD, Venkataramanan L. J Magn Reson 2002;157(1):31–42.
[42] Song YQ, Venkataramanan L, Hurlimann MD, Flaum M, Frulla P, Straley C. J Magn Reson 2002;154(2):261–8.
[43] Washburn KE, Callaghan PT. Phys Rev Lett 2006;97(17):4.
[44] McDonald PJ, Korb JP, Mitchell J, Monteilhet L. Phys Rev E 2005;72(1):011409.
[45] Monteilhet L, Korb JP, Mitchell J, McDonald PJ. Phys Rev E 2006;74(6):061404.
[46] Weber D, Mitchell J, McGregor J, Gladden LF. J Phys Chem C 2009;113 (16):6610–5.
[47] Godefroy S, Creamer LK, Watkinson PJ, Callaghan PT. The use of 2D laplace inversion in food material. In: Belton PS, Gil AM, Webb GA, Rutledge D, editors. Magnetic resonance in food science: latest developments. Cambridge, U.K: Royal Society of Chemistry; 2003.
[48] Hills B, Benamira S, Marigheto N, Wright K. Appl Magn Reson 2004;26 (4):543–60.
[49] Marigheto N, Venturi L, Hills B. Postharvest Biol Technol 2008;48(3):331–40.
[50] Venturi L, Woodward N, Hibberd D, Marigheto N, Gravelle A, Ferrante G, et al. Appl Magn Reson 2008;33(3):213–34.
[51] Chelcea RI, Fechete R, Culea E, Demco DE, Blumich B. J Magn Reson 2009;196 (2):178–90.
[52] Griffith JD, Mitchell J, Bayly AE, Johns ML. J Phys Chem B 2009;113 (20):7156–61.
[53] Marigheto N, Venturi L, Hibberd D, Wright KM, Ferrante G, Hills BP. J Magn Reson 2007;187(2):327–42.
[54] Furfaro ME, Marigheto N, Moates GK, Cross K, Parker ML, Waldron KW, et al. Appl Magn Reson 2009;35(4):521–35.
[55] Chandrasekera TC, Mitchell J, Fordham EJ, Gladden LF, Johns ML. J Magn Reson 2008;194(1):156–61.
[56] Carr HY, Purcell EM. Phys Rev 1954;94:630–8.
[57] Meiboom S, Gill D. Rev Sci Instrum 1985;29:668–91.
[58] Vold RL, Waugh JS, Klein MP, Phelps DE. J Chem Phys 1968;48:3831–2.
[59] Wilson JD. J Mater Sci 1992;27(14):3911–24.
[60] Wahba. G, Siam J. Numer Anal 1977;14(4):651–67.
[61] Hahn EL. Phys Rev 1956;80(4):580–94.
[62] Fabri D, Williams MAK, Halstead TK. Carbohydr Res 2005;340(5):889–905.
[63] Mitchell J, Griffith JD, Collins JHP, Sederman AJ, Gladden LF, Johns ML. J Chem Phys 2007;127:234701.